Published in final edited form as:

Curr Biol. 2023 July 24; 33(14): 3002–3010.e6. doi:10.1016/j.cub.2023.05.071.

Systemic coagulopathy promotes host lethality in a new *Drosophila* tumor model

Tsai-Ching Hsi[*,1], **Katy L Ong**[*,1], **Jorian J Sepers**[1,2], **Jung Kim**[1,3], **David Bilder**[1,†]

[1]Department of Molecular and Cell Biology, University of California-Berkeley, Berkeley CA, 94720, USA

SUMMARY

Malignant tumors trigger a complex network of inflammatory and wound repair responses, prompting Dvorak's characterization of tumors as 'wounds that never heal' [1]. Some of these responses lead to profound defects in blood clotting, such as Disseminated Intravascular Coagulopathy (DIC), which correlate with poor prognoses [2–4]. Here, we demonstrate that a new tumor model in *Drosophila* provokes phenotypes that resemble coagulopathies observed in patients. Fly ovarian tumors overproduce multiple secreted components of the clotting cascade and trigger hypercoagulation of fly blood (hemolymph). Hypercoagulation occurs shortly after tumor induction and is transient; it is followed by a hypocoagulative state that is defective in wound healing. Cellular clotting regulators accumulate on the tumor over time and are depleted from the body, suggesting that hypocoagulation is caused by exhaustion of host clotting components. We show that rescuing coagulopathy by depleting a tumor-produced clotting factor improves survival of tumor-bearing flies, despite the fact that flies have an open (non-vascular) circulatory system. As clinical studies suggest that lethality in patients with high serum levels of clotting components can be independent of thrombotic events [5,6], our work establishes a platform for identifying alternative mechanisms by which tumor-driven coagulopathy triggers early mortality. Moreover, it opens up exploration of other conserved mechanisms of host responses to chronic wounds.

RESULTS AND DISCUSSION

Generation of an ovarian carcinoma model to investigate tumor-host interactions

Tumor-host interactions, as well as autonomous growth of the tumor itself, play central roles in cancer progression, morbidity and mortality [7,8]. *Drosophila* has recently emerged as a valuable system to study these interactions, elucidating mechanisms that can be conserved

[†]lead contact: bilder@berkeley.edu, Lab twitter handle: @bilderlab.

[2]Current address: Division of Developmental Biology, Institute of Biodynamics and Biocomplexity, Department of Biology, Faculty of Science, Utrecht University, Padualaan 8, 3584 CH, Utrecht, The Netherlands

[3]Current Address: School of Biomedical Sciences, LKS Faculty of Medicine, The University of Hong Kong, Laboratory Block, 21 Sassoon Road, Hong Kong SAR, China

[*]equal contribution authors

AUTHOR CONTRIBUTIONS

TH, KO, and DB designed the study and wrote the manuscript. TH and KO performed most of the experiments. JJS obtained OC transcriptome data, which was managed by TH. JK and DB assisted with developing the OC fly model; JK also carried out BBB permeability assays.

DECLARATION OF INTERESTS

The authors declare no competing interests.

with mammals [9,10]. However, current systems have key limitations. In larval models, tumor-associated pupation defects prevent lifespan analysis, whereas in adult allograft models, wounding from transplantation confounds the study of the response to the tumor alone. In adult transgenic gut tumor models, perturbation of this essential organ may directly impact host metabolism, physiology, and the microbiome. We therefore developed an alternative genetic model, wherein a tumor is induced to grow in the non-essential [11] ovarian epithelium of an adult female fly (Figure 1A, S1A, B). In the ovarian carcinoma (OC) model, tumorigenesis is driven by expression of the oncogenes Ras^{V12} and $aPKC^{\Delta N}$[12], directed to the follicle epithelium via *traffic jam-Gal4 (tj-GAL4)* and restricted to adulthood via a ubiquitously expressed temperature-sensitive GAL4 repressor (*tubGAL80ts)*. This spatiotemporal control facilitates the study of both tumor and adult host from the initial stages of transformation to a fully formed malignancy.

Defining characteristics shared by mammalian and fly carcinomas include overproliferation, loss of cell polarity, and defective differentiation [7,13]. Phosphohistone H3 staining revealed elevated mitotic rates in OC cells (Figure 1B–D). Epithelial organization was strongly disrupted, as was the localization of apically and basolaterally polarized proteins (Figure 1E, F, S1C). Tumor cells failed to upregulate Hindsight (Hnt), a marker of mature differentiated follicle cells, and exhibited prolonged expression of the early follicle cell marker FasIII (Figure 1G, H) [14]. Thus, fly OC cells are transformed into malignant epithelial-derived tumors.

An additional characteristic of malignant tumors is their potential to kill hosts. Importantly, OC-bearing flies show dramatically accelerated mortality compared to controls, with median survival reduced by ~50% (Figure 1I). GAL80-mediated silencing of neural *tj-GAL4* suggests that this limited expression (Figure S2B, C H, I) is not responsible for lethality (Figure S2M, N) [15,16]. GFP labeling of oncogene-expressing cells revealed no dissemination, indicating a lack of metastasis (Figure S2A–L). Since female flies do not require ovaries to live, lethality appears to arise from systemic effects of the tumor on the host, often called paraneoplasias. Similar to other adult tumor models[17–20], OC-bearing flies exhibit bloating resulting from the accumulation of fluid in the hemocoel (Figure 1J–L). Over the course of tumorigenesis, OCs also induce reduction in fat body lipid storage (Figure 1M, N) [17–19,21]. Finally, tumor-bearing hosts displayed breakdown of the blood-brain barrier (BBB) (Figure 1O, S1F–G) [22]. The OC model therefore recapitulates previously documented *Drosophila* paraneoplasias.

To better understand OC progression and its impact on host survival, we developed a system to grade OC tumors based on distinct morphological characteristics (Figure S1C). Assessing grade was more appropriate than mass because OC tumors, particularly at early grades, contain non-transformed germline cells that are polyploid and large. We defined grade 1 tumors as exhibiting a loss of epithelial polarity and overproliferation, most evident at the poles of individual follicles, as well as beginning germline death. While grade 1 tumors do not disrupt follicle organization and transformed cells remain *in situ*, grade 2 tumors show fusion between individual follicles as well as germline absence. At grade 3, the muscle sheath and its associated basement membrane breaks down, allowing fusion between neighboring ovarioles. Further disruption of ovariole morphology resulting from organ-wide

basement membrane breakdown characterizes grade 4 tumors. Using this system, we found that tumor grade reliably increased with time after oncogene induction, and that most dying animals displayed grade 3 or 4 tumors regardless of that individual's time of death (Figure S1D, E). The accelerated host mortality driven by tumor progression in a non-essential organ in the absence of metastasis place the OC model in a unique position to study tumor-host interactions.

The OC transcriptome reveals candidate paraneoplasia mediators

To identify factors regulating these interactions, we performed bulk transcriptome analysis comparing wildtype (WT), pre-vitellogenic follicle cells to OC follicle cells 20 days after tumor induction (ATI). Expression of *matrix metalloproteinase 1* and *puckered* were increased, indicating high levels of JNK activity, as were *midline fasciclin* and *SOCS36E*, suggesting increased STAT activity (Figure 2A) [23,24]. Fluorescent reporters validated the increased activity of both pathways (Figure S2O–T), similar to other *Drosophila* epithelial tumors. *GstS1* and *Zfh1*, markers of follicle stem cells and early prefollicle cells respectively[14], were upregulated alongside downregulation of *Hnt* which marks more mature follicle cells, suggesting that some OC follicle cells retain a progenitor-like identity (Figure 2B).

Since tumor-released peptides are likely mediators of paraneoplasias, we then focused on putative secreted proteins upregulated in the OC transcriptome. Of 3567 genes showing at least 2-fold increase, 246 are predicted to encode secreted factors (Figure 2C). Several of these encode known signals overproduced by adult gut tumors as well as larval disc tumors (reviewed in [10]), including the IL-6-like Unpaireds, PDGF/VEGF-related factors, and the Insulin Growth Factor Binding Protein-like ImpL2 (Figure 2D).

Pro-clotting factors are upregulated in OC cells

Strikingly, among the upregulated genes predicted to encode secreted factors, we noted multiple genes that participate in the *Drosophila* clotting cascade (Figure 2E). As in mammals, flies have an essential circulatory fluid whose loss following wounding must be prevented. In both mammals and flies, this happens through clotting, in which soluble factors are polymerized and crosslinked to restore hemostasis [25–27]. Genes whose products in larvae form the initial 'soft clot' were overexpressed in tumor cells, including *fondue (fon), hemolectin (hml),* and *fat body protein 1 (fbp1),* which can be considered functionally analogous to human fibrin [28–30]. Some of these gene products are substrates of the fly crosslinking enzyme encoded by *transglutaminase (tg),* which is homologous to mammalian clotting factor XIIIa [31], and is also upregulated in OCs. The clotting pathway in flies includes an insect-specific reaction, called the melanization cascade[32]. This reaction is responsible for clot maturation to form a 'hard clot' and is regulated by the activity of pro-phenoloxidases (PPOs), which are released by specialized blood cells called crystal cells (CCs) following injury [32–35]. Transcript levels of *PPO1* and *PPO2* were elevated in OC cells as well. Taken together, these data raise the possibility that fly tumors may interface with the host clotting cascade.

OC tumors induce coagulopathies in hosts

We therefore asked whether coagulation is altered by OC tumors. We first measured the capacity of hemolymph from tumor-bearing adult flies to form soft clots. Adapting an assay previously used for larvae [36,37], we incubated inert Dynabeads with extracted hemolymph *ex vivo*. Hemolymph from control adults at day 5 and 10 induced clumping of beads, albeit less strongly than seen in larvae (Figure S3A–F). In striking contrast, hemolymph from OC flies 5–10 days ATI readily generated large, macroscopic bead aggregates, indicating that these animals are in a hypercoagulable state (Figure 3A, S3G, H). Aggregation activity subsequently decreases at days 15 and 20 ATI, demonstrating that the hypercoagulable state triggered by tumors is transient. The bead-clumping phenotype at day 5 represents, to our knowledge, the first demonstration of a hypercoagulation phenotype in *Drosophila* and the earliest paraneoplastic phenotype in an adult fly tumor model.

We then tested the ability of tumor-bearing hosts to create hard, melanized clots. We used two assays: first, measuring PO activity levels of hemolymph *ex vivo* on a colorimetric substrate [35,38], and second, by observing melanization of cuticular wounds *in vivo* [39]. At day 15 ATI, PO activity was decreased in tumor-bearing flies in comparison to control, and this decrease became more severe at day 20 (Figure 3B–D). Tumor-bearing flies at days 15 and 20 ATI also showed a strong failure to melanize thoracic wounds compared to control flies (Figure 3E–G). Indeed, two hours after wounding, bleeding was staunched in control flies, but hemolymph remained on the wounds of tumor-bearing flies 20 days ATI (Figure 3H). The defects in hard clotting along with wound-healing are consistent with a hypocoagulable state that follows the hypercoagulable phase.

Tumor-induced clotting creates a sink for clot cascade components

Given that hard clotting deficiencies temporally follow a period of increased soft clotting activity, we hypothesized that, as with some human paraneoplastic coagulopathies [3], fly tumors overstimulate the clotting system, leading to an exhaustion of clot components within the host. A good candidate for such a factor are CCs, which lyse to release PPOs following activation and, though produced only in the larvae, persist into adulthood [40]. Counts of circulating CCs, labelled by BcF2-GFP, in OC hosts revealed a strong decrease 15 days ATI compared to control (Figure 3I). This loss of CCs is consistent with the depletion of hemolymph PO activity and clotting failure (Figure 3B–G). Further, many BcF2-GFP-positive cells were seen on OC tissue starting at day 10 ATI, while only a few are found on control ovaries (Figure 3J–L). Transcriptional upregulation of *PPO1* (which the *BcF2-GFP* transgene reports) within OC cells, along with the failure to identify conditions for specific antibody staining of CCs, prevented unambiguous counting of tumor-associated CCs, but bright BcF2-GFP signals of sizes consistent with CCs were seen at the OC anterior. Interestingly, when the major clotting component Fon [30,41] tagged with GFP was overexpressed within the tumor, an anterior distribution of aggregated signal was seen that was distinct from the diffuse pattern seen in control ovaries (Figure 3M–O). Overall, these results suggest a model in which the OC tumor activates elements of the clotting cascade that gradually consumes essential components.

Coagulopathies driven by tumor upregulation of clotting components regulate host mortality

Finally, we asked whether coagulopathy plays a role in the premature lethality of OC flies. We tested this by using RNAi to deplete Fon, which is overproduced >25 fold in the tumor and is required for clotting in larvae [41]. Remarkably, knockdown of Fon in OC tumors extended median survival by ~38% (Figure 4A). Lifespan extension was also seen with a second, independently generated RNAi construct (Figure S4F). This extension was robust compared to control RNAis, and is of a magnitude comparable to the extension of tumor-bearing hosts seen when blood-brain barrier disruption is prevented in a different tumor model [22]. Increased lifespan correlated with reduced coagulopathy, since knocking down Fon attenuated early hypercoagulation as well as late hypocoagulation phenotypes. Quantitation revealed that hemolymph of flies bearing OC tumors depleted of Fon aggregated beads to a much lower extent than the hypercoagulative activity seen in control OC flies shortly after tumor induction (Figure 4B–D, S4A–C). At day 20 ATI, flies bearing OC tumors depleted of Fon also showed higher hemolymph PO activity and increased ability to melanize and seal wounds compared to control OC flies (Figure 4E–K, S4D, E). Thus, Fon upregulation in the tumor regulates systemic coagulopathy and paraneoplastic lethality in the host.

One explanation for coagulopathy accelerating tumor-bearing host mortality could be an autonomous effect on tumor progression. Yet quantitation of OC grade revealed no change when Fon was depleted (Figure S1H, I). A second possibility is that coagulopathy might reduce lifespan through enhancing wasting in tumor-bearing hosts. However, reducing wasting in such hosts by depletion of cachexia-inducing ImpL2 did not increase lifespan (Table S1). Fon depletion in OC flies did reduce wasting (Figure S4H–J), but without altering expression of either *ImpL2* or other potential cachexia-inducing regulators *Pvf2* and *Pvf3* (Figure S4K–M; *Pvf1* is not upregulated in OC tumors)[19]. A third possibility is that coagulopathy might accelerate host death through enhancing BBB permeability, which is a driver of tumor-associated lethality [22]. BBB breakdown was present in OC flies even upon depletion of Fon (Figure S1J). We also investigated a fourth possibility – that coagulopathy causes an elevation of ROS levels through CC release of PPOs. ROS have well-documented deleterious effects on lifespan, but also have been suggested to be at times cytoprotective [42,43]. We found that OC flies heterozygous for the *Bc* mutation, which causes premature rupture of many CCs during the larval stage, show no changes in lifespan, and OC flies carrying an engineered dominant PPO1 allele live only slightly longer than controls (Table S1) [44,45]. Treatment with antioxidant N-acetyl Cysteine or pro-oxidant Paraquat did not change OC mortality substantially, providing limited support for a role for ROS in tumor-driven mortality (Table S1). Finally, dying OC flies did not show increased intestinal permeability as detected by the ‘smurf’ assay (Figure S3I) [46]. Overall, these data suggest that coagulopathy contributes to tumor-driven death via a currently unknown paraneoplastic mechanism.

The role of individual clotting proteins in *Drosophila* larval coagulation is not well understood, and as this work is the first to interrogate adult coagulation, how the tumor-produced factors participate in this process is not yet clear. For instance, depleting *fbp1*

within the tumor caused significant lifespan extensions as did depleting *fon*, but depleting *Tg* and *hml* did not (Table S1). *fbp1* expression is normally restricted to the larval stage, so knockdown in the tumor would strongly reduce its presence in the adult host, in contrast to *tg* and *hml* which are produced by tumor-independent sources in the adult [47]. However, *fon* is also transcribed in adult fat body, yet its knockdown in the tumor alone is able to extend host lifespan. While lifespan extension of OC hosts by depletion of multiple clotting factors supports a role for coagulopathy in tumor-driven death, a mechanistic understanding of each protein's function will require further investigation.

Our data reveal an unexpected parallel between cancer patients and tumor-bearing flies: both can show widespread clotting defects that contribute to lethality. Systemic coagulopathies are common in cancer patients and have been studied since Trousseau's syndrome was described in 1865 [3,4]. One coagulopathogenic mechanism of human tumors is abnormal upregulation of Tissue Factor, which can trigger the clotting cascade [48]. Although insects do not have a similar single coagulant-initiating factor, the broad cocktail of clot-regulating proteins secreted by OC tissue suggests an analogous response in fly tumors. Indeed, to our knowledge, the data shown here reveal the first hypercoagulative phenotype documented in the fly. This adds to compelling evidence that the similar physiological reaction of metazoans to wounds and tumors has a quite ancient origin with a deeper level of conservation than previously appreciated.

Clotting complications are the second leading cause of death for cancer patients, primarily through venous thromboembolisms (VTEs) which are detected in 10–15% of all malignancies [4]. However, coagulopathy may also impact mortality through non-thrombotic pathways as well. Elevated markers of clotting factors in circulation are strongly correlated with poor survival, yet thrombosis is often not observed in patients [5,6]. There is also some evidence that prophylactic treatment with anticoagulants can improve cancer patient outcomes beyond prevention of thrombosis [49]. Thus, there may be unappreciated mechanisms through which altered clotting behavior contributes to morbidity and mortality. The fly, with its open circulatory system, is unlikely to be dying from tumor-induced thrombosis, and thus can be used as a discovery system for potential alternative mechanisms. In this work, we have not determined the exact reason why coagulopathy promotes the death of tumor-bearing flies, but our data argue against several *prima facie* feasible possibilities.

The initial hypercoagulative phenotype of OC flies followed by hypocoagulation echoes features of patient conditions such as Disseminated Intravascular Coagulopathy (DIC). DIC is considered a consumptive coagulopathy, where ectopic activation of pro-coagulation pathways can paradoxically lead to excessive bleeding through local depletion of hemostatic components[2]. Our data point to fly CCs, which lyse to provide PO clot-hardening activity, as one consumed regulator, but do not currently distinguish the relative contributions of hyper- versus hypo-coagulation to the detrimental consequences for mortality of adult tumor-bearing hosts. Future studies will explore how this simple fly system reacts to the tumor-induced danger response, perhaps by triggering inflammatory, immune, or metabolic responses that have a negative impact on host survival.

STAR Methods

RESOURCE AVAILABILITY

Lead Contact—Further information and requests for resources and reagents should be directed to and will be fulfilled by the lead contact, David Bilder (bilder@berkeley.edu).

Materials availability—Lines generated and described in this study are available on request from the Lead Contact.

Data and code availability

- Transcriptome sequencing datasets have been deposited at GEO and are publicly available as of the date of publication. Accession numbers are listed in the key resources table.
- This paper does not report original code.
- Any additional information required to reanalyze the data reported in this paper is available from the lead contact upon request.

EXPERIMENTAL MODEL AND STUDY PARTICIPANT DETAILS

Fly husbandry and stocks—Flies were maintained on cornmeal, molasses, and yeast food at 21°C in wide vials unless otherwise noted. A complete list of stocks used is given in the Key Resources Table. *fon* RNAi constructs were validated by confirming that they recapitulate previously described larval soft clotting and pupariation defects [41], as well as by qPCR (Figure S4G,H). *fbp1* RNAi was validated by qPCR (Figure S4I). *hml* RNAi was validated by confirming that it recapitulates previously described larval soft clotting defects (Figure S4J, K). *Tg* RNAi was validated by depletion of Tg protein (Figure S4L). A previously validated RNAi construct was used for *ImpL2* [21]. *fon* RNAi #2 was cloned by inserting a hairpin sequence with the sense strand GCTGCTCAGCGGAGTTCAAAC into the vector pWALIUM20. A control RNAi targeting GFP inserted a hairpin sequence with the sense strand CAAGCTGGAGTACAACTACAA into the same vector. Transgenes were created by insertion into the *attP2* site via microinjection (BestGene Inc).

METHOD DETAILS

Ovarian tumor induction and lifespan assays—After eclosion, adult females were placed with males at 21°C on food with yeast powder for two days. No more than 25 flies were kept in each wide vial. No evidence of GAL4-driven GFP expression or transformation was seen under these conditions. Flies were then moved to new food and shifted to 29°C to initiate tumor induction. Food was changed every two days and the number of dead flies was counted. For each lifespan assay, at least 90 flies were used for each sample group, with control and experimental groups assessed contemporaneously. All RNAi stocks except VALIUM20 lines from Bloomington were backcrossed at least four generations to w^{1118} (BDSC #5905) to minimize variation in genetic background. For VALIUM20 RNAi lines, control VALIUM20 lines targeting GFP were selected that were inserted at the *attP* site matching the experimental lines.

Tumor transcriptome sequencing and data analysis—Twenty days after shifting to restrictive temperature, ≥81 *tj-GAL4 tubulinGal80ts UAS-CD8::GFP* and ≥26 *tj-GAL4 tubulinGa80ts UAS-CD8::GFP; UAS-aPKCΔN UAS-RasV12* ovaries were dissected in Schneider's *Drosophila* Media (Life Technologies, 21720024) on ice for each biological replicate. Two biological replicates were sequenced per genotype. Follicles ~stage 6 and older of control ovaries were removed by cutting the distal regions. Ovaries were washed three times in DPBS (Dulbecco's Phosphate-buffered saline; Life Technologies, 14190144) followed by 10 minute incubation in 10mg/mL *Bacillus licheniformis* protease (Sigma, P5380) prepared in DPBS at 6°C while vigorously agitating. Protease activity was quenched by adding a half volume of 10% fetal bovine serum (FBS) in Schneider's *Drosophila* Media. Cell suspension was then filtered using a 50μm filter (Sysmex Partec, 04-004-2327) to remove germ cells, and the filtered suspension was subsequently spun down for 7 minutes at 1000g. Cell viability was assessed by Trypan Blue dye (Sigma, T8154). RNA of pelleted cells was isolated using RNeasy mini kit (QIAGEN, 74104), and RNA quantity and quality was analyzed by the Functional Genomics Laboratory at the California Institute for Quantitative Biosciences at UC Berkeley (QB3-Berkeley). Libraries were sequenced by 50bp single-end reads on HiSeq4000 platform (Illumina, San Diego, CA), and sequencing was performed by the Vincent J. Coates Genomics Sequencing Lab at QB3-Berkeley. Sequences were aligned to the *Drosophila melanogaster* reference genome (version 6.26) using Kallisto under default parameters for single-end reads [50]. Lowly expressed genes were removed prior to differential expression analysis using DESeq2 [51].

Immunofluorescence—Ovarian tumors, thoracic muscle, brains and intestines were dissected in PBS and fixed in 4% PFA-PBS for one hour at room temperature without agitation. Samples were washed three times with PBS-TX (0.1% Triton-X in 1X PBS) before proceeding to dye treatment. Samples were blocked in 2% BSA or 4% NGS/1% BSA blocking solution for 30–60 minutes. Primary antibodies were incubated overnight at 4°C and used at the following concentrations: anti-Dlg (1:100), anti-phospho-histone H3 (1:250), and anti-Hindsight (1:100). Samples were washed three times with PBS-TX and incubated with AlexaFluor-conjugated secondary antibodies for 1 hour at room temperature. Tissues were again washed three times with PBS-TX prior to additional chemical staining. To stain actin, fixed tissues were incubated for 30–60 minutes at room temperature with Rhodamine-Phalloidin at a concentration of 1:500. To stain nuclei, a 1:1000 DAPI solution was applied for 10 minutes. After all incubations, samples were washed three times with PBS and incubated in the final wash for at least 20 minutes. Samples were mounted in Diamond Antifade Mountant before imaging.

Visualizing fat body wasting—Dorsal cuticles were dissected from adult flies in PBS and fixed in 4% PFA for 30 minutes. Samples were washed once in PBS-TX and three times in PBS. Dorsal cuticles were incubated in Nile Red staining solution (0.5 μg/mL in 1X PBS) for 10 minutes followed by three washes in PBS. Samples were then stained with DAPI, then mounted in Diamond Antifade Mountant and stored at 4°C. Images were taken at multiple focal planes on Zeiss Axio Imager M2 using Zeiss Zen (blue edition 2.3) pro imaging software, and multifocus images were created using Helicon Focus 7.

PO activity measurements—We used a modified protocol from Sorrentino et al [38]. To measure PO activity of hemolymph *ex vivo*, individual flies were bled onto small squares of Whatman filter paper (1cm^2; Whatman 1001 – Grade 1). Immediately following each bleeding, 20μL of 20mM L-DOPA in PBS was applied to each blot. Samples were then covered to prevent evaporation and incubated for 30 minutes at 25°C. The blots were rapidly dried by heating in a microwave for 10 seconds and then allowed to completely air-dry for 30 minutes. Following drying, each blot was sealed in clear Scotch tape and scanned using an Epson Perfection 4490 Photo Scanner. Intensity of each blot was quantified in FIJI, and the mean background intensity was subtracted from all samples.

Thoracic wound healing assay—Flies were anesthetized with CO_2, and one side of the thorax was punctured using a blunt 0.005 inch diameter tungsten needle (Ted Pella #27–11). Flies were then returned to vials, and two hours later counted for melanized thoracic wounds using a dissecting microscope. To determine wound-healing failure, a glass micropipette tip (World Precision Instruments #TIP30TW1) was gently brought into contact with the thoracic wound two hours after wounding, and assessed for whether hemolymph was drawn up by capillary action.

Bead aggregation assay—We used a modified protocol from Kucerova et al [37]. Dynabeads were washed with 10X PBS twice and blocked in a 0.1% BSA-PBS solution overnight on a rotator at 4°C. The beads were washed three times with 0.1X PBS and reconstituted in Ringer's-PTU (130mM NaCl, 5mM KCl, 1.5mM $CaCl_2 \times 2H_2O$, 2mM Na_2HPO_4, 0.37mM KH_2PO_4, 0.01% PTU) buffer at a final concentration of 50%. The blocked beads were stored up to two weeks on a rotator at 4°C. To extract hemolymph, we used a modified protocol from Troha et al [52]. A Qiagen spin column was disassembled and the filter paper removed. All other components were rinsed in MilliQ purified water. The column was reassembled without the filter and centrifuged at 13.2 × 1000g for 10 minutes at room temperature. The tube that the column was nested in was replaced with a fresh 1.5mL Eppendorf tube. Flies were anesthetized and shallowly cut across the dorsal thorax with a 33G needle. The flies were transferred to the modified column stored on ice. All flies were wounded in less than 10 minutes to avoid loss of clotting activity. The column was spun at 5000g for 5min at 4°C. 2μL of hemolymph was combined with 2uL of blocked beads in a well of a 15-well glass slide by pipetting up and down ten times. The slide was incubated in a humid chamber at 25°C for 30minutes. Bead aggregates were revealed by swirling the solution with a 10μL micropipette tip for 30 seconds. The well was photographed with an iPhone 12 camera with a 1.6 aperture wide lens mounted on a dissecting microscope. To observe aggregation at higher magnification, an upright Zeiss Axio Imager M2 with a Ph 1 Plan-Neofluar 10x/0.30 objective was used to image samples in bright field. To measure bead aggregation, we used the Bernsen Adaptive Local Thresholding Method available in FIJI to generate a binary image. A polygon was drawn around the liquid droplet and the percent area unoccupied by beads (i.e. the white area) was measured. The final measurement was generated after subtracting the average white area percent measured across five wells of control reactions with 2μL of Ringer's-PTU buffer instead of hemolymph.

qPCR—RNA was isolated with a Qiagen RNeasy minikit from 3 whole wandering L3 larvae; 150 ovaries and 30 tumors were prepped as for RNA-sequencing above. At least three biological replicates were collected for each sample type. cDNA was generated with an iScript cDNA synthesis kit. cDNA was diluted 1:10 and qPCR was performed with SsoAdvanced Universal SYBR Green Super Mix on an Applied Biosystems Step One Plus. *Rp49* was used as a reference gene control. Primer sequences are listed in the Key Resources Table. The ΔΔCT method was used to quantify relative expression and statistical testing was performed on the ΔΔCT values to determine significance.

Western Blot—8 whole larvae were homogenized in 50μL lysis buffer (10mM Tris-Hcl, 150mM NaCl, 0.5mM EDTA, 0.5% NP-40 with protease inhibitor) on ice. The sample was spun for 10 minutes at 16,000g to remove tissue debris. The BCA assay was performed on the supernatant to measure total protein. Protein lysates were combined with 4X Laemli loading buffer and boiled for 10 minutes. 10 μg of protein was separated by SDS-PAGE and transferred to PVDF membranes. Membranes were blocked with 3% BSA in TBS-Tween for 30 minutes and incubated with primary antibodies (1:2,000 anti-Tg A/B and 1:20,000 anti-Beta Tubulin) overnight at 4°C[53]. After washing with TBS-T, the membrane was incubated at room temperature with 1:10,000 of HRP-conjugated secondary antibodies. After a final wash, bound antibody was revealed with WesternBright chemiluminscent detection reagents.

Hemocyte bleeds—Adult hemocyte bleeding protocol was modified from Boulet et al [54]. Individual flies were bled in a droplet of 1X PBS on a poly-D-lysine coated glass bottom dish (MatTek Life Sciences P35G-1.5-14-C) by flushing flies three times using a hand-pulled glass pipette (World Precision Instruments 1B100-4). Cells were allowed to settle for at least 15 minutes and were then fixed in 4% PFA for 15 minutes at room temperature. Fixed samples were counterstained with DAPI and mounted in antifade mountant. BcF2-GFP positive crystal cells were manually counted on a Zeiss Axio Imager M2.

Confocal microscopy—Fixed samples were imaged on the Zeiss LSM700 Scanning Confocal Microscope with a Plan-APOCHROMAT 20x/0,8 objective. The microscope was controlled with Zeiss Zen 2010 imaging software. Images were processed and analyzed with FIJI software.

Blood brain barrier permeability assay—Assays were done as described in Kim et al [22]. Approximately 100nL of 25 mg/ml 10,000 MW TR-dextran was injected in the abdomen of adult females using a fine glass needle. If tumor-bearing hosts excreted hemolymph upon injection due to bloating, excess hemolymph was removed. 15 hours after injection, flies were fixed in 4% PFA-PBS for 80 minutes and washed in 0.1% PBS-TX before brain dissection. Brains were imaged on the same day of fixation to minimize diffusion of dextran. Average intensity was measured in a cross-section at the center of the brain at two regions using FIJI software.

Drug Treatments—Paraquat was used at 5mM. N-Acetyl Cysteine (NAC) was administered at 20mM. All drugs were dissolved in MilliQ-filtered water. 0.74g of 4–24 Carolina Instant Blue Food was mixed with 2mL of water or drug cocktail. Drugged

food was always made fresh the day of use. Paraquat treatment was started 6 days after tumor induction. After two days, flies were transferred to food reconstituted with water, and thereafter consistently alternated every two days between Paraquat food and water only food. This alternating treatment was done to avoid Paraquat-driven mortality [55,56]. NAC treatment was begun 10 days after tumor induction to avoid potential delays in early tumorigenesis from the antioxidant treatment.

Water weight measurements—Measurements were done as described in Denholm et al [57]. Briefly, four to five flies were placed into a 1.5mL centrifuge tube, and wet weight was measured on Mettler Toledo AG104 scale. Flies were then dried at 65°C overnight with the centrifuge tube opened to allow for evaporation. Dry weight was then measured. Water weight was obtained by subtracting the dry weight measurement from the wet weight measurement, and the result was divided by the number of flies in the respective tube.

Smurfing Assay—The smurfing assay was carried out as described in Rera et al [46]. In brief, flies were moved onto food containing 2.5% wt/vol Blue Dye No. 1. After 9 hours, the flies with dye present outside of the digestive tract were counted.

QUANTIFICATION AND STATISTICAL ANALYSIS

Image Analysis—Maximum projections of Fon::GFP and BcF2-GFP images were created for measurement in FIJI software. Projections were thresholded to create binary images and the anterior end of the control ovary or tumor was selected using the freehand selection tool. Analyze particles was used to count the number of GFP+ particles, with the minimum particle size set to $5\mu m^2$ and $25\mu m^2$ respectively for Fon::GFP and BcF2-GFP.

Statistics—A two-way ANOVA test or Student's T-test was used for parametric data (crystal cell counts, PO activity, bead aggregation, water weight, fluorescent microscopy data, and qPCR). The Mann-Whitney U test, Kruskal-Wallis test or Fisher's exact test was used for non-parametric data (wound melanization, tumor grading, bleeding defects and smurf assay). Correlation between grade and time ATI was determined by calculating Kendall's τ_b correlation coefficient. The Log-Rank test was used to determine significant differences in survival curves. Graphpad Prism and Python were used to perform statistical testing. All error bars on graphs show SEM.

Supplementary Material

Refer to Web version on PubMed Central for supplementary material.

ACKNOWLEDGEMENTS

We acknowledge Ulrich Theopold for sharing Drosophila clotting expertise, and Yuejiang Liu for technical assistance. Iswar Hariharan, Lin He, Daniel Nomura and Shaina Carroll provided many helpful discussions. We thank Sravya Gadepalli for assisting in lifespan assays for the final revision of this manuscript. Reagents were generously gifted by Bruno Lemaitre, Robert Schulz, Shun-ichiro Kawabata, Katja Brueckner, Elisabeth Knust and the community resources by the Vienna Drosophila Resource Center and the Bloomington Drosophila Stock Center. This work has been supported by NIH grants GM130388 and GM090150 to DB, a University of California Cancer Research Coordinating Fellowship to TH, and a Mark Foundation-Damon Runyon Fellowship 2400–20 to KO.

REFERENCES

1. Dvorak HF (1986). Tumors: Wounds that do not heal. N Engl J Med 315, 1650–1659. [PubMed: 3537791]
2. Levi M, and ten Cate H (1999). Disseminated Intravascular Coagulation. N Engl J Med 341, 586–592. [PubMed: 10451465]
3. Levi M (2009). Disseminated intravascular coagulation in cancer patients. Best Pract Res Clin Haematol 22, 129–136. 10.1016/j.beha.2008.12.005. [PubMed: 19285279]
4. Khorana AA (2010). Venous thromboembolism and prognosis in cancer. Thromb Res 125, 490–493. 10.1016/j.thromres.2009.12.023. [PubMed: 20097409]
5. Krenn-Pilko S, Langsenlehner U, Stojakovic T, Pichler M, Gerger A, Kapp KS, and Langsenlehner T (2015). An elevated preoperative plasma fibrinogen level is associated with poor disease-specific and overall survival in breast cancer patients. Breast 24, 667–672. 10.1016/j.breast.2015.08.003. [PubMed: 26346586]
6. Marchetti MR, Masci G, Santoro A, de Braud F, Celio L, Labianca R, Mandalà M, Merelli B, Tondini C, Gasparini G, et al. (2014). Hypercoagulation Screening As a Marker of Thrombosis and Poor Disease Prognosis in Cancer Patients: The Hypercan Prospective Study. Blood 124, 586–586. 10.1182/blood.v124.21.586.586.
7. Hanahan D, and Weinberg RA (2011). Hallmarks of cancer: The next generation. Cell 144, 646–674. 10.1016/j.cell.2011.02.013. [PubMed: 21376230]
8. McAllister SS, and Weinberg RA (2014). The tumour-induced systemic environment as a critical regulator of cancer progression and metastasis. Nat Cell Biol 16, 717–727. 10.1038/ncb3015. [PubMed: 25082194]
9. García-López L, Adrados I, Ferres-Marco D, and Dominguez M (2021). A blueprint for cancer-related inflammation and host innate immunity. Cells 10. 10.3390/cells10113211.
10. Bilder D, Ong K, Hsi TC, Adiga K, and Kim J (2021). Tumour–host interactions through the lens of Drosophila. Nat Rev Cancer 21, 687–700. 10.1038/s41568-021-00387-5. [PubMed: 34389815]
11. Komitopoulou K, Gans M, Margaritis LH, Kafatos FC, and Masson M (1983). Isolation and Characterization of Sex-Linked Female-Sterile Mutants in Drosophila Melanogaster With Special Attention To Eggshell Mutants. Genetics 105, 897–920. 10.1093/genetics/105.4.897. [PubMed: 17246182]
12. Betschinger J, Mechtler K, and Knoblich JA (2003). The Par complex directs asymmetric cell division by phosphorylating the cytoskeletal protein Lgl. Nature 422, 326–330. 10.1038/nature01486. [PubMed: 12629552]
13. Bilder D (2004). Epithelial polarity and proliferation control: Links from the Drosophila neoplastic tumor suppressors. Genes Dev 18, 1909–1925. 10.1101/gad.1211604. [PubMed: 15314019]
14. Rust K, Byrnes LE, Yu KS, Park JS, Sneddon JB, Tward AD, and Nystul TG (2020). A single-cell atlas and lineage analysis of the adult Drosophila ovary. Nat Commun 11. 10.1038/s41467-020-19361-0.
15. Jukam D, Xie B, Rister J, Terrell D, Charlton-Perkins M, Pistillo D, Gebelein B, Desplan C, and Cook T (2013). Opposite feedbacks in the Hippo pathway for growth control and neural fate. Science (1979) 342. 10.1126/science.1238016.
16. Weaver LN, Ma T, and Drummond-Barbosa D (2020). Analysis of Gal4 expression patterns in adult drosophila females. G3: Genes, Genomes, Genetics 10, 4147–4158. 10.1534/g3.120.401676.
17. Figueroa-Clarevega A, and Bilder D (2015). Malignant drosophila tumors interrupt insulin signaling to induce cachexia-like wasting. Dev Cell 33, 47–56. 10.1016/j.devcel.2015.03.001. [PubMed: 25850672]
18. Kwon Y, Song W, Droujinine IA, Hu Y, Asara JM, and Perrimon N (2015). Systemic organ wasting induced by localized expression of the secreted Insulin/IGF antagonist ImpL2. Dev Cell 33, 36–46. 10.1016/j.devcel.2015.02.012. [PubMed: 25850671]
19. Song W, Kir S, Hong S, Hu Y, Wang X, Binari R, Tang HW, Chung V, Banks AS, Spiegelman B, et al. (2019). Tumor-Derived Ligands Trigger Tumor Growth and Host Wasting via Differential MEK Activation. Dev Cell 48, 277–286.e6. 10.1016/j.devcel.2018.12.003. [PubMed: 30639055]

20. Gateff E, and Schneiderman HA (1969). Neoplasms in mutant and cultured wild-type tissues of Drosophila. Natl Cancer Inst Monogr 31, 365–397. [PubMed: 5374686]
21. Ding G, Xiang X, Hu Y, Xiao G, Chen Y, Binari R, Comjean A, Li J, Rushworth E, Fu Z, et al. (2021). Coordination of tumor growth and host wasting by tumor-derived Upd3. Cell Rep 36, 109553. 10.1016/j.celrep.2021.109553. [PubMed: 34407411]
22. Kim J, Chuang HC, Wolf NK, Nicolai CJ, Raulet DH, Saijo K, and Bilder D (2021). Tumor-induced disruption of the blood-brain barrier promotes host death. Dev Cell 56, 2712–2721.e4. 10.1016/j.devcel.2021.08.010. [PubMed: 34496290]
23. Bina S, Wright VM, Fisher KH, Milo M, and Zeidler MP (2010). Transcriptional targets of Drosophila JAK/STAT pathway signalling as effectors of haematopoietic tumour formation. EMBO Rep 11, 201–207. 10.1038/embor.2010.1. [PubMed: 20168330]
24. la Marca JE, and Richardson HE (2020). Two-Faced: Roles of JNK Signalling During Tumourigenesis in the Drosophila Model. Front Cell Dev Biol 8, 1–20. 10.3389/fcell.2020.00042. [PubMed: 32117956]
25. Furie B, and Furie BC (1988). The Molecular Basis of Blood Coagulation. Cell 53, 505–518. [PubMed: 3286010]
26. Ariëns RAS, Lai TS, Weisel JW, Greenberg CS, and Grant PJ (2002). Role of factor XIII in fibrin clot formation and effects of genetic polymorphisms. Blood 100, 743–754. 10.1182/blood.V100.3.743. [PubMed: 12130481]
27. Theopold U, Krautz R, and Dushay MS (2014). The Drosophila clotting system and its messages for mammals. Dev Comp Immunol 42, 42–46. 10.1016/j.dci.2013.03.014. [PubMed: 23545286]
28. Scherfer C, Karlsonn C, Loseva O, Bidla G, Goto A, Havemann J, Dushay MS, and Theopold U (2004). Isolation and Characterization of Hemolymph Clotting Factors in Drosophila melanogaster by a Pullout Method. Current Biology 14, 625–629. 10.1016/j. [PubMed: 15062105]
29. Karlsson C, Korayem AM, Scherfer C, Loseva O, Dushay MS, and Theopold U (2004). Proteomic analysis of the Drosophila larval hemolymph clot. Journal of Biological Chemistry 279, 52033–52041. 10.1074/jbc.M408220200. [PubMed: 15466469]
30. Lindgren M, Riazi R, Lesch C, Wilhelmsson C, Theopold U, and Dushay MS (2008). Fondue and transglutaminase in the Drosophila larval clot. J Insect Physiol 54, 586–592. 10.1016/j.jinsphys.2007.12.008. [PubMed: 18222466]
31. Wang Z, Wilhelmsson C, Hyrsl P, Loof TG, Dobes P, Klupp M, Loseva O, Mörgelin M, Iklé J, Cripps RM, et al. (2010). Pathogen entrapment by transglutaminase - A conserved early innate immune mechanism. PLoS Pathog 6. 10.1371/journal.ppat.1000763.
32. Tang H (2009). Regulation and function of the melanization reaction in Drosophila. Fly (Austin) 3, 105–111. 10.4161/fly.3.1.7747. [PubMed: 19164947]
33. Rizki TM, Rizki RM, and Bellotti RA (1985). Genetics of a Drosophila phenoloxidase. MGG Molecular & General Genetics 201, 7–13. 10.1007/BF00397978.
34. Bidla G, Lindgren M, Theopold U, and Dushay MS (2005). Hemolymph coagulation and phenoloxidase in Drosophila larvae. Dev Comp Immunol 29, 669–679. 10.1016/j.dci.2004.11.007. [PubMed: 15854679]
35. Bidla G, Dushay MS, and Theopold U (2007). Crystal cell rupture after injury in Drosophila requires the JNK pathway, small GTPases and the TNF homolog eiger. J Cell Sci 120, 1209–1215. 10.1242/jcs.03420. [PubMed: 17356067]
36. Lesch C, Goto A, Lindgren M, Bidla G, Dushay MS, and Theopold U (2007). A role for Hemolectin in coagulation and immunity in Drosophila melanogaster. Dev Comp Immunol 31, 1255–1263. 10.1016/j.dci.2007.03.012. [PubMed: 17509683]
37. Kucerova L, Broz V, Arefin B, Maaroufi HO, Hurychova J, Strnad H, Zurovec M, and Theopold U (2016). The Drosophila Chitinase-Like Protein IDGF3 Is Involved in Protection against Nematodes and in Wound Healing. J Innate Immun 8, 199–210. 10.1159/000442351. [PubMed: 26694862]
38. Sorrentino RP, Small CN, and Govind S (2002). Quantitative analysis of phenol oxidase activity in insect hemolymph. Biotechniques 32, 815–823. 10.2144/02324st08. [PubMed: 11962604]

39. Dudzic JP, Kondo S, Ueda R, Bergman CM, and Lemaitre B (2015). Drosophila innate immunity: Regional and functional specialization of prophenoloxidases. BMC Biol 13, 1–16. 10.1186/s12915-015-0193-6. [PubMed: 25555396]
40. Banerjee U, Girard JR, Goins LM, and Spratford CM (2019). Drosophila as a genetic model for hematopoiesis. Genetics 211, 367–417. 10.1534/genetics.118.300223. [PubMed: 30733377]
41. Scherfer C, Qazi MR, Takahashi K, Ueda R, Dushay MS, Theopold U, and Lemaitre B (2006). The Toll immune-regulated Drosophila protein Fondue is involved in hemolymph clotting and puparium formation. Dev Biol 295, 156–163. 10.1016/j.ydbio.2006.03.019. [PubMed: 16690050]
42. Nam HJ, Jang IH, You H, Lee KA, and Lee WJ (2012). Genetic evidence of a redox-dependent systemic wound response via Hayan protease-phenoloxidase system in Drosophila. EMBO Journal 31, 1253–1265. 10.1038/emboj.2011.476. [PubMed: 22227521]
43. Lennicke C, and Cochemé HM (2020). Redox signalling and ageing : insights from Drosophila. 48, 367–377.
44. Neyen C, Binggeli O, Roversi P, Bertin L, Sleiman MB, and Lemaitre B (2015). The Black cells phenotype is caused by a point mutation in the Drosophila pro-phenoloxidase 1 gene that triggers melanization and hematopoietic defects1Equal contribution.1. Dev Comp Immunol 50, 166–174. 10.1016/j.dci.2014.12.011. [PubMed: 25543001]
45. Lanot R, Zachary D, Holder F, and Meister M (2001). Postembryonic Hematopoiesis in Drosophila. Dev Biol 230, 243–257. 10.1006/dbio.2000.0123. [PubMed: 11161576]
46. Rera M, Clark RI, and Walker DW (2012). Intestinal barrier dysfunction links metabolic and inflammatory markers of aging to death in Drosophila. Proc Natl Acad Sci U S A 109, 21528–21533. 10.1073/pnas.1215849110. [PubMed: 23236133]
47. Li H, Janssens J, de Waegeneer M, Kolluru SS, Davie K, Gardeux V, Saelens W, David FPA, Brbić M, Spanier K, et al. (2022). Fly Cell Atlas: A single-nucleus transcriptomic atlas of the adult fruit fly. Science (1979) 375. 10.1126/science.abk2432.
48. Kasthuri RS, Taubman MB, and Mackman N (2009). Role of tissue factor in cancer. Journal of Clinical Oncology 27, 4834–4838. 10.1200/JCO.2009.22.6324. [PubMed: 19738116]
49. Green D, Hull RD, Brant R, and Pineo GF (1992). Lower mortality in cancer patients treated with low-molecular-weight versus standard heparin. The Lancet 339, 1476. 10.1049/cce:20050511.
50. Bray NL, Pimentel H, Melsted P, and Pachter L (2016). Near-optimal probabilistic RNA-seq quantification. Nat Biotechnol 34, 525–527. 10.1038/nbt.3519. [PubMed: 27043002]
51. Love MI, Huber W, and Anders S (2014). Moderated estimation of fold change and dispersion for RNA-seq data with DESeq2. Genome Biol 15, 8–9. 10.1186/s13059-014-0550-8.
52. Troha K, and Buchon N (2019). Methods for the study of innate immunity in Drosophila melanogaster. Wiley Interdiscip Rev Dev Biol 8, 2–3. 10.1002/wdev.344.
53. Shibata T, Ariki S, Shinzawa N, Miyaji R, Suyama H, Sako M, Inomata N, Koshiba T, Kanuka H, and Kawabata SI (2010). Protein crosslinking by transglutaminase controls cuticle morphogenesis in Drosophila. PLoS One 5. 10.1371/journal.pone.0013477.
54. Boulet M, Renaud Y, Lapraz F, Benmimoun B, Vandel L, and Waltzer L (2021). Characterization of the Drosophila Adult Hematopoietic System Reveals a Rare Cell Population With Differentiation and Proliferation Potential. Front Cell Dev Biol 9, 1–17. 10.3389/fcell.2021.739357.
55. Rzezniczak TZ, Douglas LA, Watterson JH, and Merritt TJS (2011). Paraquat administration in Drosophila for use in metabolic studies of oxidative stress. Anal Biochem 419, 345–347. 10.1016/j.ab.2011.08.023. [PubMed: 21910964]
56. Bonilla-Ramirez L, Jimenez-Del-Rio M, and Velez-Pardo C (2013). Low doses of paraquat and polyphenols prolong life span and locomotor activity in knock-down parkin Drosophila melanogaster exposed to oxidative stress stimuli: Implication in autosomal recessive juvenile Parkinsonism. Gene 512, 355–363. 10.1016/j.gene.2012.09.120. [PubMed: 23046578]
57. Denholm B, Hu N, Fauquier T, Caubit X, Fasano L, and Skaer H (2013). The tiptop/teashirt genes regulate cell differentiation and renal physiology in Drosophila. Development (Cambridge) 140, 1100–1110. 10.1242/dev.088989.

58. Gajewski KM, Sorrentino RP, Lee JH, Zhang Q, Russell M, and Schulz RA (2007). Identification of a Crystal Cell-Specific Enhancer of the Black Cells Prophenoloxidase Gene in Drosophila. Genesis 45, 200–207. 10.1002/dvg. [PubMed: 17417793]

59. Chatterjee N, and Bohmann D (2012). A versatile φC31 based reporter system for measuring AP-1 and NRF2 signaling in Drosophila and in tissue culture. PLoS One 7. 10.1371/journal.pone.0034063.

60. Firmino J, Tinevez JY, and Knust E (2013). Crumbs Affects Protein Dynamics In Anterior Regions Of The Developing Drosophila Embryo. PLoS One 8. 10.1371/journal.pone.0058839.

61. Green N, Odell N, Zych M, Clark C, Wang ZH, Biersmith B, Bajzek C, Cook KR, Dushay MS, and Geisbrecht ER (2016). A common suite of coagulation proteins function in drosophila muscle attachment. Genetics 204, 1075–1087. 10.1534/genetics.116.189787. [PubMed: 27585844]

62. Chakrabarti S, and Visweswariah SS (2020). Intramacrophage ROS Primes the Innate Immune System via JAK/STAT and Toll Activation. Cell Rep 33, 108368. 10.1016/j.celrep.2020.108368. [PubMed: 33176146]

63. Xu C, Luo J, He L, Montell C, and Perrimon N (2017). Oxidative stress induces stem cell proliferation via TRPA1/RyR-mediated Ca2+signaling in the Drosophila midgut. Elife 6, 1–24. 10.7554/eLife.22441.

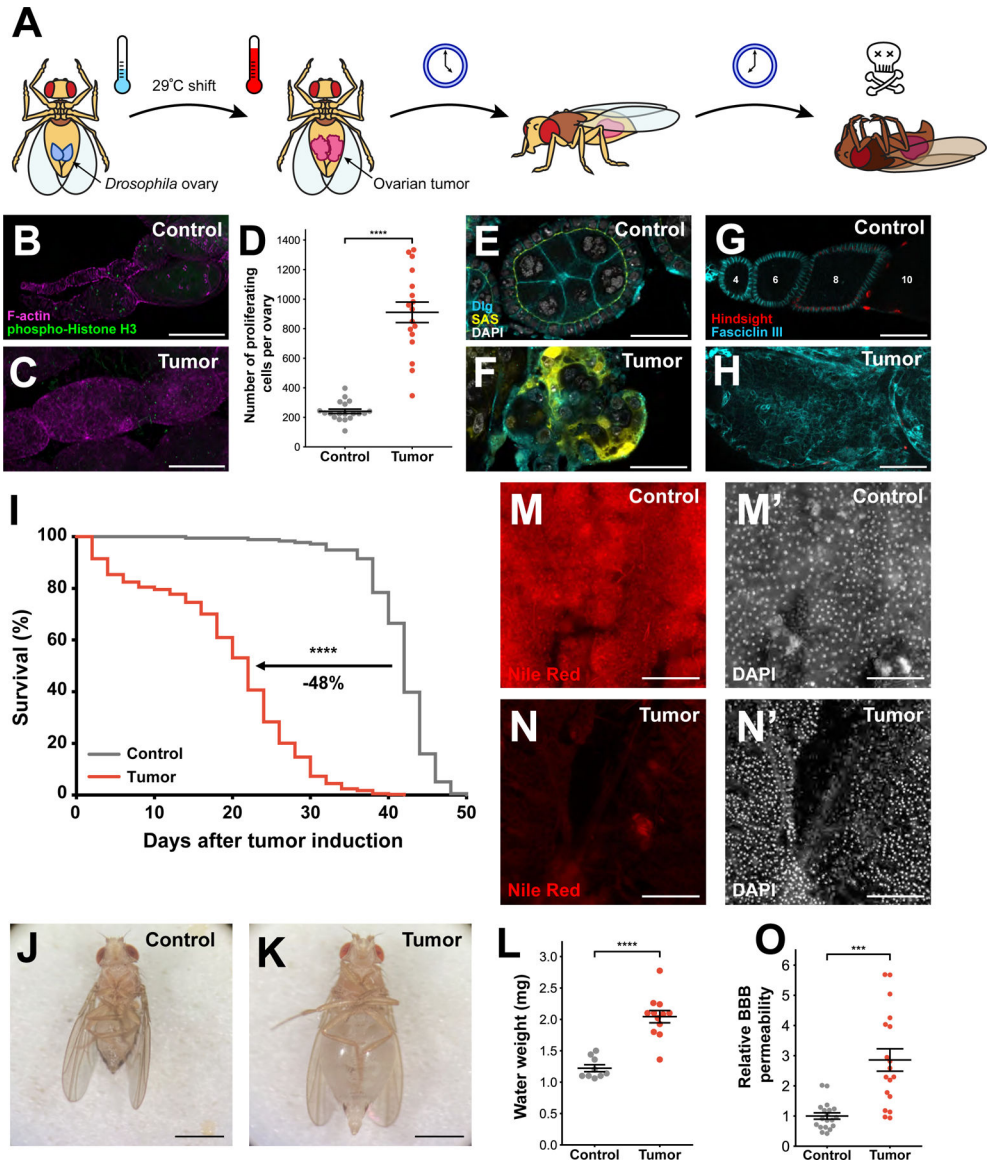

Figure 1. A novel ovarian carcinoma model to study paraneoplasias in Drosophila.

(A) Schematic of *Drosophila* ovarian carcinoma (OC) induction in adult flies. (B, C) OC tumors exhibit increased anti-phospho-histone H3 staining (green, Max Z-projections), quantitated in (D, n-values: Control=19, Tumor=17). (E, F) Apical SAS::Venus (yellow) and lateral anti-Dlg staining (cyan) reveal disruption of cellular organization in transformed follicle epithelial cells (n-values: Control=3, Tumor=7). (G, H) OC tumors fail to differentiate into the mature Hnt-positive (red), FasIII-negative (cyan) follicles of control; numbers in G represent follicle stages (n-values: Control=10, Tumor=14). (I) Flies carrying OCs (n=176) have greatly reduced survival compared to control, non-tumor-bearing flies (n=338). Tumor-bearing flies exhibit substantial fluid accumulation as indicated by abdomen distention (J, K, n-values: Control=39, Tumor=70) and quantification of water weight (L, n-values: Control=9, Tumor=12). (M, N) Lipid staining (red) shows decreased fat tissue in OC flies (Control mean grey value=767.13±28.01 au, n=10; Tumor mean grey

value=458.97±69.50 au, n=18; p=0.0011). (O) OC flies exhibit increased permeability of the blood-brain barrier (n-values: Control=19, Tumor=18). Scale Bars = 100μm (B, C), 50μm (G, H), 25μm (E, F), 1mm (J, K), 250μm (M, N); Error bars = S.E.M; Two-tailed t-test (D, L, O) and log-rank test (I) used to determine significance; *p < .05, ***p < .0005, ****p < .00005. Dots in (L) represent pools of 4–5 flies, (O) represent individual flies. See also Figure S1, S2 and Table S1, S2.

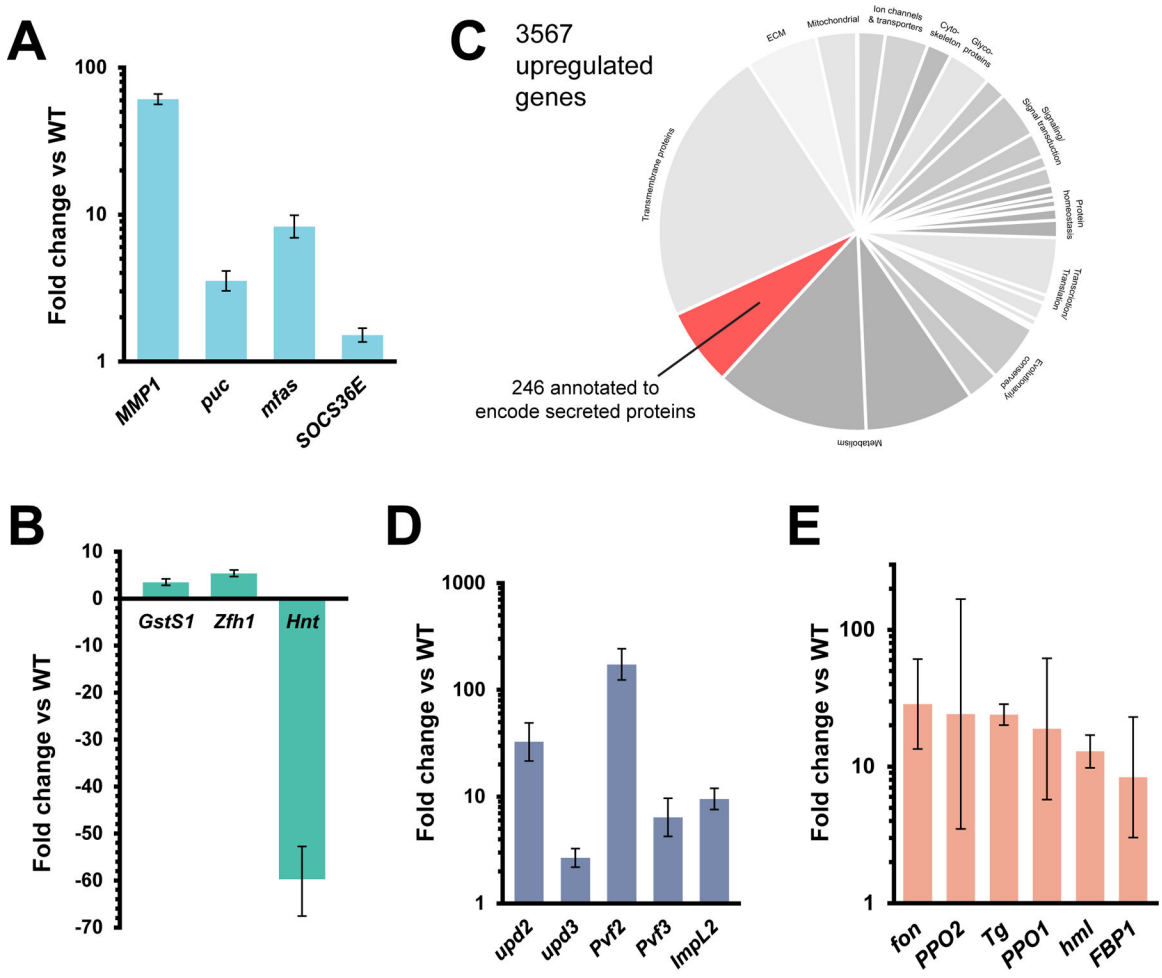

Figure 2. OCs differentially express clotting factors and regulators, among a number of other secreted proteins.

(A) OCs exhibit heightened transcription of JNK pathway targets *MMP1* (60.97X, p<0.0005) and *puc* (3.53X, $p=3.68\times10^{-15}$), as well as STAT pathway targets *mfas* (8.28X, $p=6.59\times10^{-32}$) and *SOCS36E* (1.52X, $p=4.53\times10^{-4}$). (B) Increased proportion of OC tumor cells in early differentiation is indicated by enhanced transcript levels of *GstS1* (3.45X, 4.73×10^{-10}) and *Zfh1* (5.35X, $p=5.35\times10^{-38}$), and the failure to upregulate *hnt* (-59.71X, $p=5.28\times10^{-237}$). (C) 246 of 3567 transcripts upregulated in OC tumors vs control follicles are predicted to encode secreted proteins. (D) Like other *Drosophila* tumors, OCs upregulate *upd2* (32.58X, $p=1.95\times10^{-16}$) and *upd3* (2.68X, $p=3.34\times10^{-6}$), *Pvf2* (173.00X, $p=8.82\times10^{-52}$), *Pvf3* (6.41X, $p=2.47\times10^{-5}$), and *ImpL2* (9.54X, $p=1.16\times10^{-21}$). (E) Expression of many factors associated with hemolymph clotting are increased in OCs compared to wild-type follicle cells: *fon* (28.58X, $p=3.75\times10^{-5}$), *hml* (12.89X, 2.97×10^{-19}), *Tg* (23.92X, $p=1.15\times10^{-69}$), *PPO1* (18.84X, p=0.0296), *PPO2* (24.22X, p=0.169), and *FBP1* (8.35X, p=0.07). Two biological replicates were generated for RNA-sequencing analysis. Error bars = S.E.M. See also Figure S2 and Table S1, S2.

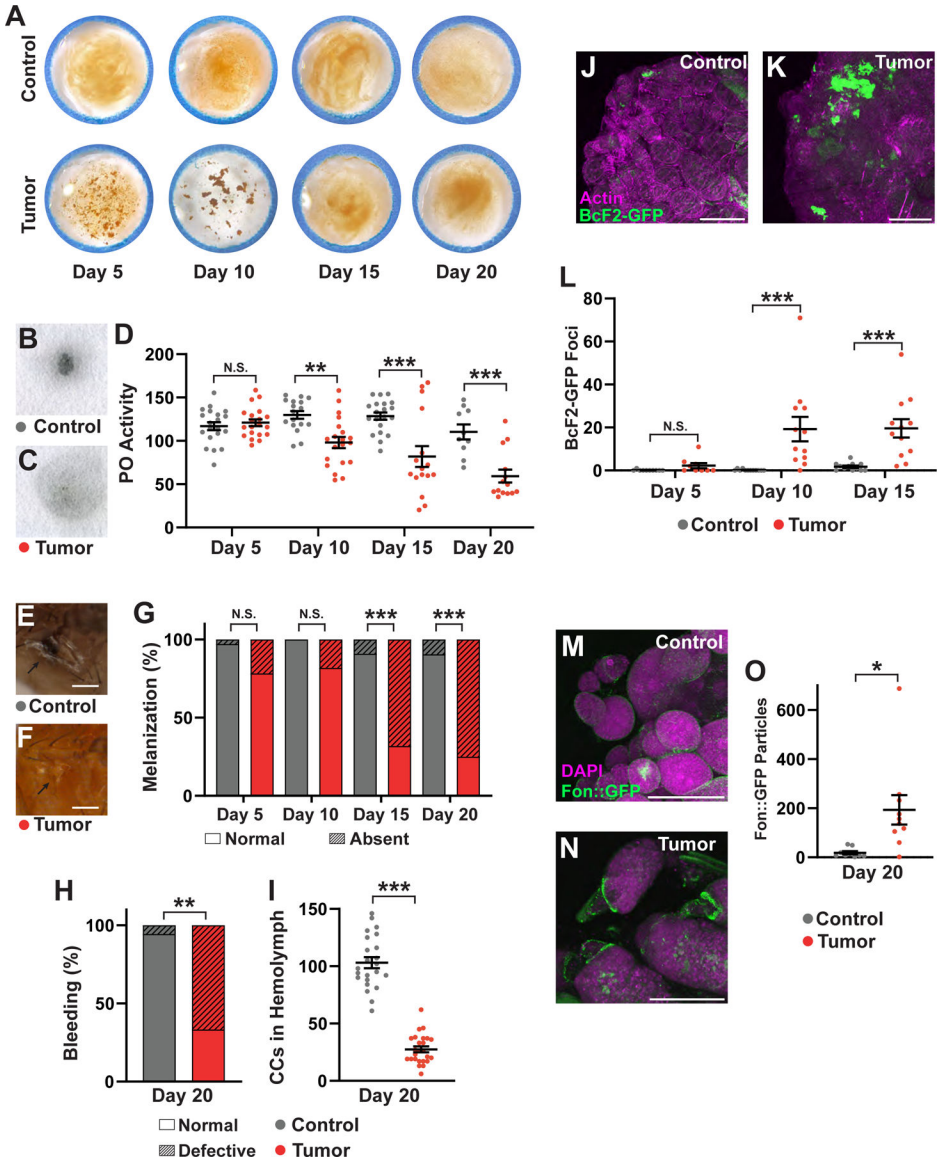

Figure 3: Drosophila ovarian tumors induce multiple defects in clotting.

(A) Bead aggregation assay shows that soft clotting activity, which is low in control adult hemolymph (top), is dramatically increased in OC adult hemolymph (bottom) through day 10 AT. Images are representative of ≥3 biological replicates and do not come from a single time course. PO activity in control (B) and OC flies (C) measured by L-DOPA blot reactivity. (D) Quantification of PO activity reveals decreases in OC flies following 10 days ATI (n≥10 for each group). Thoracic wound response in control (E) and OC flies (F). (G) Percentage of flies able to melanize wounds reveals strong differences on days 15 and 20 ATI (n≥22 for each group). (H) Hypocoagulation of OC flies, demonstrated by ability to extract hemolymph from thoracic wounds after 2 hours (n-values: Control=18, Tumor=9). (I) Compared to control (n=23), BcF2-positive crystal cell counts in hemolymph decrease in tumor-bearing flies (n=25) at day 20 ATI. Only a few BcF2-positive cells are found on control ovaries (J) compared to several dozen on ovarian tumors day 15 ATI

(K); quantitated in (L, n≥10 for each group). A Fon::GFP fusion protein expressed in control ovaries (M) shows diffuse signal, whereas the same fusion protein expressed in OC cells shows particulate aggregation (N). Quantitated in (O, n ≥9). (J, K, M, N) show maximum-projected images. Scale Bars = 250μm (E,F), 100μm (I,J,M,N); Error bars = S.E.M.; Two-way ANOVA (D, L), Fisher's Exact test (G, H) and student's T-test (I, O) used to determine significance; *p < .05, **p < .005, ***p < .0005, N.S. = not significant. Dots in (D) and (I) represent individual flies, (L) and (O) represent individual ovaries. See also Figure S3, Table S2.

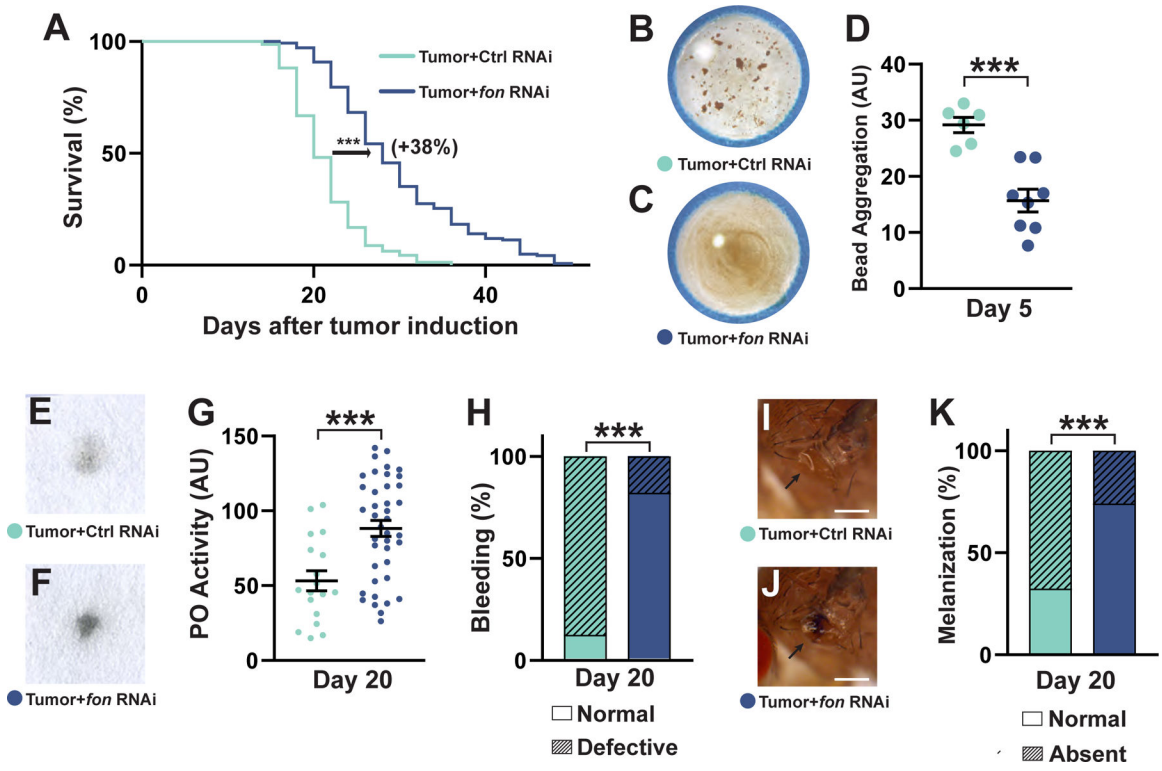

Figure 4: Tumor-secreted Fondue drives coagulopathies and early mortality.

(A) Early mortality induced by OC tumors is significantly reduced upon Fon depletion (n-values: Ctrl RNAi=160, *fon* RNAi=142). Compared to control RNAi depletion in OC cells (B), Fon depletion in OC cells (C) rescues the strong hypercoagulation displayed by tumor-bearing flies, revealed by the bead aggregation assay and quantitated in (D, n-values: Ctrl RNAi=6, *fon* RNAi=8). Compared to control RNAi expression in OC cells (E), Fon depletion in OC cells (F) also ameliorates the loss of PO activity, quantitated in (G, n-values: Ctrl RNAi=18, *fon* RNAi=40), defects in bleeding (H, n-values: Ctrl RNAi=8, *fon* RNAi=45) and wound melanization (I-K, n-values: Ctrl RNAi=75, *fon* RNAi=122). Scale Bars = 25μm; Error bars = S.E.M.; Log-rank test (A), student's T-test (D, G), and Fisher's Exact test (H, K) used to determine significance; *p < .05, ***p < .0005. Dots in (D) represent 2 ul of hemolymph pooled from ≥20 flies, (G) represent individual flies. See also Figure S1, S3, S4 and Table S1, S2.

Key resources table

REAGENT or RESOURCE	SOURCE	IDENTIFIER
Antibodies		
Mouse Anti-Dlg	Developmental Studies Hybridoma Bank	4F3
Anti-phospho-Histone H3	Cell Signaling	9701
Mouse Anti-hindsight	Developmental Studies Hybridoma Bank	1G9
Anti-Transglutaminase A/B	*Shibata et al.*[53]	PMID 20976106
Bacterial and virus strains		
none		
Biological samples		
none		
Chemicals, peptides, and recombinant proteins		
TRITC-Phalloidin	Sigma-Aldrich	P1951
DAPI	ThermoFisher Scientific	D1306
Nile Red	Sigma-Aldrich	N3013
Paraformaldehyde 16%	Electron Microscopy Sciences	15710
Phosphate Buffered Solution	Sigma-Aldrich	P4417
Triton-X	Sigma-Aldrich	T8787
Phenylthiourea	Sigma-Aldrich	P7629
L-DOPA	Sigma-Aldrich	D9628
Dynabeads M-280 Tosylactivated	Invitrogen	14203
Formula 4-24 Instant Drosophila Medium	Carolina Biological Supply Company	173210
Bovine Serum Albumin	Sigma Aldrich	A3912
10 kDa Texas red-Dextran	ThermoFisher Scientific	D1863
SlowFade Diamond Antifade Mount	Invitrogen	S36963
TWEEN 20	Sigma-Aldrich	P9416
NaCl	Fisher Chemical	S271
KCl	Fisher Chemical	P217
$CaCl_2 \times 2H_2O$	Fisher Chemical	C79
Na_2HPO_4	Fisher Chemical	S374
KH_2PO_4	Fisher Chemical	P284
Paraquat	Sigma-Aldrich	36541
N-Acetyl-L-Cysteine	Sigma-Aldrich	A7250
Alexa Fluor Phalloidin 647	Invitrogen	A22287
Schneider's *Drosophila* Medium	Gibco	21720-024
Dulbecco's Phosphate-buffered saline	Gibco	14190144
Protease from *Bacillus licheniformis*	Sigma-Aldrich	P5380
Fetal bovine serum	Cytiva Life Sciences	SH30070.03
RNeasy mini kit	QIAGEN	74104

REAGENT or RESOURCE	SOURCE	IDENTIFIER
Poly-D-Lysine	MilliporeSigma	A003E
SsoAdvanced Universal SYBR Green Supermix	Bio-Rad	1725271
iScript cDNA Synthesis Kit	Bio-Rad	1708891
Pierce BCA Protein Assay Kit	Thermo Scientific	23225
Tris Base	Fisher Chemical	BP152-500
Nonidet P40	Roche Diagnostics	1754599
EDTA	Sigma-Aldrich	E9884
Tris-HCl	Fisher Chemical	BP153-500
Critical commercial assays		
none		
Deposited data		
Transcriptome data: control ovaries and ovary tumors (two replicates for each genotype)	This paper	GEO: GSE 207849
Experimental models: Cell lines		
none		
Experimental models: Organisms/strains		
w^{1118}	Bloomington Drosophila Stock Center	5905
BcF2-GFP	*Gajewski et al.*[58]	FBal0244649
BcF6-GFP	*Gajewski et al.*[58]	FBal0244650
UAS-Fondue #1 RNAi	Vienna Drosophila Resource Center	330748
UAS-Fondue #2 RNAi	This study	n/a
UAS-Hml RNAi	Bloomington Drosophila Stock Center	50640
UAS-Tg RNAi	Bloomington Drosophila Stock Center	65086
UAS-FBP1 RNAi	Vienna Drosophila Resource Center	330200
UAS-ImpL2 RNAi	Bloomington Drosophila Stock Center	64936
10XSTAT-GFP	Bloomington Drosophila Stock Center	26198
AP1-RFP	*Chatterjee & Bohmann*[59]	FBal0268835
Vkg::GFP	Vienna Drosophila Resource Center	318167
tj-GAL4	Kyoto Stock Center	104055
UAS-aPKC$^{\Delta N}$	Bloomington Drosophila Stock Center	51673
UAS-Ras^{V12}	Bloomington Drosophila Stock Center	4847
Fasciclin III::GFP trap line	Bloomington Drosophila Stock Center	#59809
Tub-GAL80^{ts}	Bloomington Drosophila Stock Center	7109
UAS-SAS::Venus	*Firmino et al.*[60]	FBtp0084565
UAS-NLS::GFP	Bloomington Drosophila Stock Center	4776
UAS-Fon::GFP	Bloomington Drosophila Stock Center	43646
UAS-CD8::GFP	Liqun Luo	FBti0012685
UAS-GFP #1 RNAi	Vienna Drosophila Resource Center	60201
UAS-GFP #2 RNAi	Bloomington Drosophila Stock Center	41552

REAGENT or RESOURCE	SOURCE	IDENTIFIER
UAS-GFP #3 RNAi	Bloomington Drosophila Stock Center	41553
UAS-GFP #4 RNAi	This study	n/a
UAS-RFP RNAi	Bloomington Drosophila Stock Center	67852
nSyb-GAL80	Bloomington Drosophila Stock Center	92154
Daughterless-GAL4	Bloomington Drosophila Stock Center	55850
Oligonucleotides		
FON FW primer: GTCCCCACTTCCGAGTATTACA	*Green et al.*[61]	PMID 27585844
FON REV primer: CCTCGTGATGAACGTAACGCT	*Green et al.*[61]	PMID 27585844
RP49 FW primer: GCCCAAGGGTATCGACAACA	*Green et al.*[61]	PMID 27585844
RP49 REV primer: GCGCTTGTTCGATCCGTAAC	*Green et al.*[61]	PMID 27585844
FBP1 FW primer: CTTCGCCGTAATGTGGTCTAC	*Chakrabati & Visweswariah*[62]	PMID 33176146
FBP1 REV primer: GAGCTTGAGTGTCCTCACGA	*Chakrabati & Visweswariah*[62]	PMID 33176146
IMPL2 FW primer: AAGAGCCGTGGACCTGGTA	*Kwon et al.*[18]	PMID 25850671
IMPL2 Rev primer: TTGGTGAACTTGAGCCAGTC	*Kwon et al.*[18]	PMID 25850671
PVF2 FW primer: GGTGGTCCACATCACGAGAG	*Xu et al.*[63]	PMID 28561738
PVF2 REV primer: CGACTTTGTCGCTGCATC	*Xu et al.*[63]	PMID 28561738
PVF3 FW primer: TCGTGAAGAGCAGTAAGCATCG	*Xu et al.*[63]	PMID 28561738
PVF3 REV primer: AGGTGCAACTCAGTATGGTGG	*Xu et al.*[63]	PMID 28561738
Recombinant DNA		
pWALIUM20 Vector	Drosophila Genomics Resource Center	1472
Software and algorithms		
FIJI	ImageJ	http://fiji.sc
Zeiss Imaging Software (Zen)	Zeiss	www.zeiss.com/microscopy/us/products/microscope-software/zen.html
Kallisto Alignment Software	Pachter Lab	https://pachterlab.github.io/kallisto/
R Statistical Software	The R Foundation	n/a
Graphpad	Prism	Ver 9.3.1
Gene List Annotation for Drosophila	DRSC/TRiP Functional Genomics Resources	https://www.flyrnai.org/tools/glad/web/
Python	Python Software Foundation	Ver 3.9.7
Helicon Focus 7	Helicon Soft Limited	Ver 7.7.5
Other		
15-well slides	MP Biomedicals	096041505
Pre-pulled glass pipette -- 30 μm diameter	World Precision Instruments	TIP30TW1
Borosilicate glass capillaries	World Precision Instruments	1B100-4
50 μm filter	Sysmex Partec	04-004-2327
Qiaprep 2.0 Spin Columns	QIAGEN	27115
35mm glass bottom petri dish (No. 1.5 coverglass)	MatTek Life Sciences	P35G-1.5-14-C

REAGENT or RESOURCE	SOURCE	IDENTIFIER
Mini Protean TGX Pre-cast Protein Gel, 7.5%	Bio-Rad	4561023
Amersham Hybond 0.45 PVDF Blotting Membrane	GE Healthcare Life Science	10600023
96-well PCR Plate	Thermo Scientific	AB0700
Microseal ‘B’ Seals	Bio-Rad	MSB1001